

Graphical Abstract

STEI-PCN: an efficient pure convolutional network for traffic prediction via spatial-temporal encoding and inferring

Kai Hu, Zhidan Zhao, Zhifeng Hao

Highlights

STEI-PCN: an efficient pure convolutional network for traffic prediction via spatial-temporal encoding and inferring

Kai Hu, Zhidan Zhao, Zhifeng Hao

- Achieved a balanced configuration of the respective capture ranges for the three types of correlations under their synergistic effect.
- Proposed a new multi-view collaborative predicting module.

STEI-PCN: an efficient pure convolutional network for traffic prediction via spatial-temporal encoding and inferring

Kai Hu^a, Zhidan Zhao^{b,c,*}, Zhifeng Hao^a

^a*Department of Mathematic, School of Mathematics and Computer Sciences, Shantou University, Shantou, 515063, Guangdong, China*

^b*Department of Computer Science, School of Mathematics and Computer Sciences, Shantou University, Shantou, 515063, Guangdong, China*

^c*Complexity Computation Laboratory, Department of Computer Science, School of Mathematics and Computer Sciences, Shantou University, Shantou, 515603, Guangdong, China*

Abstract

Traffic data exhibits complex temporal, spatial, and spatial-temporal correlations. Capturing and integrating these correlations is crucial for building accurate prediction models. Although numerous deep learning-based traffic prediction models have been developed, most of these models use either independent modules to separately extract temporal and spatial correlations or joint modules to synchronously extract them, without considering the spatial-temporal correlations. Moreover, models that consider joint spatial-temporal correlations (temporal, spatial, and spatial-temporal correlations) often encounter significant challenges in accuracy and computational efficiency which prevent such models from demonstrating the expected advantages of a joint spatial-temporal correlations architecture. To address these issues, this paper proposes an efficient pure convolutional network for traffic prediction via spatial-temporal encoding and inferring (STEI-PCN). The model introduces and designs a dynamic adjacency matrix inferring module based on absolute spatial and temporal coordinates, as well as relative spa-

*Corresponding author at: Department of Computer Science, School of Mathematics and Computer Sciences, Shantou University, Shantou, 515063, Guangdong, China and Complexity Computation Laboratory, Department of Computer Science, School of Mathematics and Computer Sciences, Shantou University, Shantou, 515603, Guangdong, China.

Email address: zzhidanzhao@gmail.com (Zhidan Zhao)

tial and temporal distance encoding, using a graph convolutional network combined with gating mechanism to capture local synchronous joint spatial-temporal correlations. Additionally, three layers of temporal dilated causal convolutional network are used to capture long-range temporal correlations. Finally, through multi-view collaborative prediction module, the model integrates the gated-activated original, local synchronous joint spatial-temporal, and long-range temporal features to achieve comprehensive prediction. This study conducts extensive experiments on flow datasets (PeMS03/04/07/08) and speed dataset (PeMS-Bay), covering multiple prediction horizons. The results show that STEI-PCN demonstrates competitive computational efficiency in both training and inference speeds, and achieves superior or slightly inferior to state-of-the-art (SOTA) models on most evaluation metrics.

Keywords: Traffic prediction, Synchronous joint spatial-temporal correlations, Graph convolutional network, Temporal dilated causal convolution

1. Introduction

The surge in transportation vehicles poses significant challenges to traffic networks, such as congestion [1, 2, 3]. Intelligent Transportation Systems (ITS) are a crucial solution [4], with numerous traffic data (*e.g.*, flow, speed, etc.) from traffic networks providing a robust data foundation [5]. Real-time perception and accurate traffic prediction are central to ITS, enhancing transportation safety, reducing congestion, and optimizing travel [6]. These capabilities make it a key research area in both academia and industry.

Traffic prediction aims to predict future traffic states by analyzing historical traffic data and the structure of traffic networks. However, accurately predicting future traffic states is a challenging task due to the inherently complex and nonlinear nature of traffic networks, as well as the intricate correlations within traffic data [7, 8, 9]. Traffic networks exhibit a typical spatial-temporal graph structure [10], with three types of correlations among the traffic states of nodes. Temporal correlations: The traffic states of nodes display significant periodicity. As shown in Fig. 1(a), the traffic flow data collected by *Sensor20* generally exhibit a clear daily periodic pattern (*e.g.*, repetitive patterns during morning and evening peaks, etc.). However, short-term incidents such as traffic accidents can cause abrupt fluctuations in flow, increasing the difficulty of long-term prediction [11, 12]. Spatial correlations:

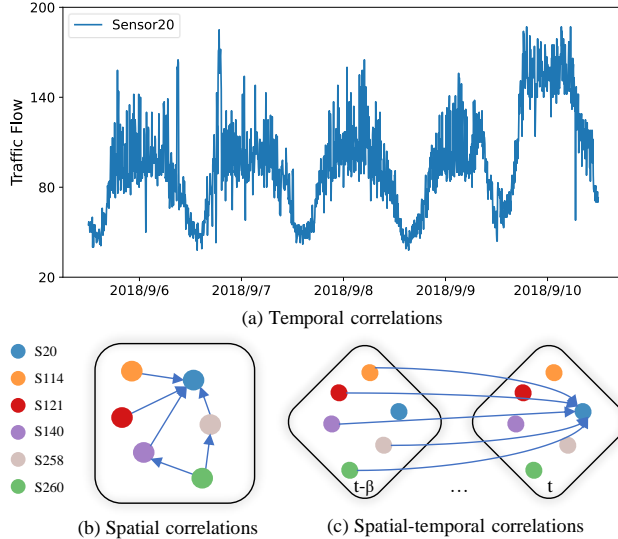


Figure 1: Illustration of three types of correlations.

The traffic states of a node are not only influenced by its own spatial location but also significantly depend on the states of its upstream and downstream neighboring nodes. As shown in Fig. 1(b), the traffic states of *Senor20* are affected not only by its directly connected neighbors but also by the indirect influence of more distant neighbors [12]. Spatial-temporal correlations: The traffic states of a node can be influenced by the past states of its neighboring nodes. As shown in Fig. 1(c), the traffic states of *Sensor20* are influenced not only by the potential impact of its neighbors at timestamp $t - 1$ but also by the potential impact of neighbors at earlier timestamps, up to $t - \beta$. Capturing and integrating these correlations is crucial for building accurate prediction models.

Although numerous deep learning-based traffic prediction models have been developed, most models employ a decoupled architecture, where temporal and spatial correlations are extracted separately by independent modules [12, 13, 14] or they use joint modules to synchronously extract temporal and spatial correlations [15, 16, 17], but fail to consider spatial-temporal correlations. Moreover, models that consider joint spatial-temporal correlations (incorporating temporal, spatial, and spatial-temporal correlations) [18, 19, 20, 21] often face bottlenecks in accuracy and computational efficiency (refer to the evaluation metrics and training or inference times pro-

vided in the original papers), failing to demonstrate the superiority of the joint spatial-temporal correlations architecture. For example, on the PeMS03 dataset, the decoupled architecture model GWN [14] still maintains a leading position compared to them.

This study employs a architecture that combines local synchronous joint spatial-temporal correlations with long-range temporal correlations to build our model. This choice stems from the following considerations: the traffic states of a node are influenced by both short-term and long-term temporal sequences of observations, as well as by the interactive influence of past and current states of neighboring nodes in the spatial dimension. However, an excessively large range of spatial and spatial-temporal correlations can introduce noise, negatively impacting prediction performance. Therefore, the model design needs to balance the capture range of local and global features [22] to achieve a balance between prediction accuracy and robustness. Building a model using this architecture requires addressing three key issues:

- Design of the synchronous joint spatial-temporal correlations module: Some modules use attention-based methods to capture joint spatial-temporal correlations synchronously, such as ConSTGAT [18], which encodes temporal, spatial, and spatial-temporal information, concatenates and reshapes the resulting vectors for information fusion, and finally uses attention mechanisms to capture synchronous joint spatial-temporal correlations. However, this method faces issues of weak interpretability and reliance on prior information, limiting its application in new traffic networks. Therefore, designing a lightweight module that can capture dynamic synchronous joint spatial-temporal correlations while maintaining high interpretability is a key problem that current research needs to address.
- Utilization of spatial and temporal position and distance information: The interaction relationships between nodes exhibit significant dynamic characteristics, and this dynamism is influenced by the most intuitive factors of position and distance. Using static pre-defined spatial distance graphs [12, 23, 24] or traffic data similarity graphs [25] to model spatial-temporal relationships cannot effectively capture the real-time impact of position and distance factors on the dynamic interactions between nodes. Therefore, developing a weight modeling mechanism that dynamically reflects the influence of spatial and temporal position and distance is of great significance for improving model accuracy.

- Fusion of multiple features: Methods that directly generate predictions by simply adjusting the output channels or use multi-layer capture components in the temporal correlations and concatenate their outputs before feeding them into a linear layer to generate predictions (*e.g.*, DST-GraphSAGE [20], etc.) have obvious limitations: They fail to fully consider the differential contributions and complementary information of original, local synchronous joint spatial-temporal, and long-range temporal features to the prediction results. Therefore, developing a new fusion mechanism that can effectively balance and integrate multi-view features is of great significance for improving the accuracy and robustness of prediction models.

We propose a new solution to the above problems by introducing a single-layer graph convolutional network (GCN) based on the joint spatial-temporal graph A_{STP} [19] to capture local dynamic synchronous joint spatial-temporal correlations. Combining with three layers of temporal dilated causal convolutional network (TDCN) [26] to explicitly capture long-range temporal correlations, and using a multi-view collaborative predicting module (MVC) to provide more comprehensive prediction capabilities. Finally, we construct an efficient pure convolutional network for traffic prediction via spatial-temporal encoding and inferring (STEI-PCN), suitable for both short-term and long-term traffic prediction. The main contributions of this paper are as follows:

- We propose an efficient pure convolutional network for traffic prediction via spatial-temporal encoding and inferring (STEI-PCN), which uses a single-layer GCN based on the joint spatial-temporal graph A_{STP} [19] to capture local dynamic synchronous joint spatial-temporal correlations and employs TDCNs to capture long-range temporal correlations, ensuring a highly parallelized computation process and significantly improving computational efficiency. Through hyperparameters tuning, a balanced configuration of the respective capture ranges of the three correlations is achieved under synergistic interaction.
- We design a polynomial function-based inference component STEI, which uses spatial and temporal position and distance encoding to infer the dynamic adjacency matrix of the joint spatial-temporal graph. Compared to the inference component STPRI [19], the number of parameters is reduced from $12d$ to $6d$, and the computational complexity

is reduced from $O(d^2)$ to $O(d)$, significantly improving the computational efficiency of the synchronous joint spatial-temporal correlations module.

- We propose a multi-view collaborative predicting module (MVC), which integrates original, local synchronous joint spatial-temporal, and long-range temporal features to provide more comprehensive prediction capabilities.
- We conduct extensive experiments on four traffic flow datasets and one speed dataset. The results show that STEI-PCN controls the parameter scale at a reasonable level (around 0.46M) and exhibits extremely fast training and inference speeds, demonstrating competitive computational efficiency. Moreover, STEI-PCN performs superiorly or slightly inferiorly to state-of-the-art (SOTA) models on most evaluation metrics across all prediction horizons in the datasets.

2. Related works

2.1. Traffic predicting models using temporal and spatial correlations

We summarize several models that integrate temporal and spatial correlations. These can be primarily categorized into two major classes: models based on decoupled architecture, including static graph models, dynamic graph models, and non-graph-structured models. And models that use joint modules to extract synchronous temporal and spatial features.

In static graph models, DCRNN [12] employs GCN to extract spatial correlations while using recurrent neural network (RNN) to capture temporal correlations. Similarly, STGCN [13] utilizes GCN to process spatial features and temporal convolutional network (TCN) to extract temporal features. GMAN [23] separately processes temporal and spatial features based on graph attention mechanisms. PDFformer [24] and RGDAN [27] achieve the extraction of temporal and spatial features by combining embedding mechanisms with graph attention mechanisms. However, static graph models have inherent limitations in effectively capturing the dynamic evolution characteristics of traffic networks [28]. To overcome these limitations, researchers have proposed dynamic graph-based models. ASTGCN [29] uses GCN to extract spatial features, CNN to process temporal features, and introduces attention mechanisms to enhance model performance. GWN [14]

and MTGNN [30] both employ GCN to extract spatial features and TCN to process temporal features. AGCRN [31], DSTAGNN [32], and DGCRN [33] adopt a combination of GCN and RNN, with DSTAGNN further incorporating attention mechanisms. Z-GCNETs [34] uses a pure GCN structure to separately extract temporal and spatial features. HTVGNN [35] combines GCN with attention mechanisms to handle temporal and spatial features. Additionally, some studies have explored non-graph-structured modeling approaches. STNorm [36] employs regularization mechanisms for modeling. STEP [37] applies a pre-training strategy and utilizes transformers for downstream prediction tasks. STD-MAE [38] uses an encoder-decoder structure to separately process temporal and spatial features. STID [39] and STAEformer [40] both adopt embedding mechanisms, with STID using linear layers to separately extract temporal and spatial features, while STAEformer implements feature extraction based on attention mechanisms. DTRformer [41] is entirely built on attention mechanisms.

Models that extract synchronous features use joint modules to simultaneously capture temporal and spatial correlations. STSGCN [15] constructs local synchronous spatial-temporal graph by connecting nodes to themselves across adjacent timestamps and utilizes the aggregation mechanism of GCN to synchronously extract local temporal and spatial correlations. However, STSGCN is limited to modeling local temporal and spatial correlations. In contrast, STFGNN [16] generates similarity graphs based on node feature similarities and integrates them into a unified spatial-temporal fusion graph, enabling the simultaneous capture of both local and global temporal and spatial correlations. Furthermore, STFGNN introduces a gated convolutional module to effectively capture long-range temporal and spatial correlations, significantly enhancing the ability to model complex spatial and temporal patterns. T-Graphormer [17] is a transformer-based model that incorporates temporal dynamics into the Graphormer architecture, allowing each node to attend to all other nodes in the graph sequence, thereby simultaneously modeling spatial and temporal correlations. This design enables the model to capture rich spatial and temporal patterns with minimal reliance on pre-defined spatial-temporal inductive biases.

2.2. Traffic predicting models using joint spatial-temporal correlations

We focus on describing several models that take into account joint spatial-temporal correlations. Models based on the joint spatial-temporal correlations architecture primarily face two core challenges: First, how to effec-

tively extract correlations features across the temporal, spatial, and spatial-temporal dimensions. Secondly, how to integrate and synergistically utilize these three types of correlations features.

Some models use decoupled architecture to separately extract temporal, spatial, and spatial-temporal correlations, and employ different fusion methods to integrate these features. DST-GraphSAGE [20] utilizes a spatial-temporal GraphSAGE module to generate spatial-temporal embeddings from the historical observations of a node’s spatial neighbors, thereby extracting local spatial-temporal correlations. Simultaneously, it integrates an attention mechanism into the model to dynamically learn spatial correlations between traffic nodes based on graph features. Additionally, it stacks four layers of TDCN in the temporal convolutional layer to capture long-range temporal correlations in traffic data. Finally, the output of each TDCN is activated using gated linear units (GLU) [42], concatenated and passed through a 1×1 convolutional layer to adjust the output shape to obtain the final prediction. SSGCRTN [21] proposes a spatial-specific graph convolution operation to identify patterns unique to each spatial dimension, thereby extracting spatial correlations. For spatial-temporal correlations, it introduces a spatial-temporal interaction module that integrates multi-granularity spatial-temporal information of nodes. This module learns and utilizes spatial-temporal correlations between different time points from both forward and reverse perspectives, revealing hidden patterns in spatial-temporal associations. Furthermore, it employs a transformer-based global temporal fusion module to capture global temporal correlations. Finally, the attention features are concatenated, normalized using layer normalization to improve model convergence, and passed through a fully connected neural network layer to perform linear transformations on the output sequence for the final prediction.

Some models use joint modules to simultaneously extract temporal, spatial, and spatial-temporal correlations. Among them, implicit relationship learning models based on attention mechanisms implicitly learn synchronous joint spatial-temporal correlations between nodes through spatial-temporal attention weights. The core idea is to design adaptive attention mechanisms to filter key joint spatial-temporal contexts. ConSTGAT [18] encodes temporal, spatial, and spatial-temporal information, concatenates and reshapes the resulting encoding vectors for information fusion, and uses attention mechanisms to capture synchronous joint spatial-temporal correlations. However, this method faces issues of weak interpretability and reliance on prior infor-

mation, limiting its application in new traffic networks. In contrast, explicit topology models based on GCN construct joint spatial-temporal graphs to encode joint spatial-temporal relationships into graph structures, leveraging the neighborhood aggregation mechanism of GCN to explicitly capture synchronous joint spatial-temporal correlations. STPGCN [19] achieves synchronous modeling of local temporal, spatial, and spatial-temporal correlations by constructing a local joint spatial-temporal graph A_{STP} . Based on this, it generates encoding vectors for nodes’ spatial and temporal positions as well as spatial and temporal distances between nodes. Subsequently, it proposes a spatial-temporal position-aware relation inference module (STPRI) to adaptively infer the weights of the three important correlations. The generated local joint spatial-temporal relationships are then integrated into the graph convolutional layers for aggregating and updating node features. Additionally, a spatial-temporal position-aware gating activation unit (STPGAU) is designed in the graph convolution, guiding the capture of node-specific pattern features through position embeddings. By stacking three layers of graph convolutional networks, the model indirectly captures global synchronous joint spatial-temporal correlations. Finally, the features from each graph convolutional layer are concatenated, passed through the MLP, and adjusted in shape to obtain the final prediction. The strength of this method lies in its highly interpretable structure, where the local joint spatial-temporal graph A_{STP} simultaneously models the three correlations, aligning with the evolution patterns of traffic states. However, this method has significant limitations: capturing long-range synchronous joint spatial-temporal correlations indirectly through stacking multiple layers of graph convolutional networks not only reduces computational efficiency but also exacerbates the feature smoothing problem [43], while making it difficult to achieve an effective balance between local and global feature extraction for the three correlations. Nevertheless, the innovative aspects of this method greatly inspired us. In our model, we introduce and improve this synchronous joint spatial-temporal correlations module, significantly enhancing computational efficiency. Through architectural and modular innovations, we address these existing limitations, demonstrating more competitive computational efficiency and accuracy in experiments.

3. Preliminaries

3.1. Traffic network

A traffic network can be represented by a directed or undirected graph, denoted by $G = (V, E, A)$. Here, $V = \{v_1, v_2, \dots, v_N\}$ is a set of traffic nodes, and $E \subseteq \{(v_i, v_j) \mid v_i, v_j \in V \wedge i \neq j\}$ contains edges between neighboring nodes. Let $d(v_i, v_j)$ be the edge counting function, which counts the minimum number of edges traversed from v_i to v_j . For a given node v_i , its k th-order neighbor set is defined as $N_i(k) = \{v_j \mid d(v_i, v_j) = k, j = 1, \dots, N\}$, with $N_i(0)$ denoting the node itself. To represent the connectedness of nodes in G , the adjacency matrix $A \in \mathbb{R}^{N \times N}$ is defined with each element $A_{i,j} = 1$ if $(v_i, v_j) \in E$ and 0 otherwise.

3.2. Problem description

Traffic forecasting aims to predict future traffic data at multiple nodes in a traffic road network based on their historical observations. Given a traffic road graph G , we use $X = [X_1, \dots, X_T] \in \mathbb{R}^{T \times N \times 1}$ to denote a type of traffic data (flow or speed) generated at N nodes over T time steps, where X_t represents the traffic data at time step $t \in \{1, \dots, T\}$. The traffic flow forecasting problem can be formulated as follows: Given historical traffic data $X = [X_{t-T_h+1}, \dots, X_t]$ over T_h time steps, the task is to predict the future traffic data $X^P = [X_{t+1}, \dots, X_{t+T_p}]$ over T_p time steps by learning a mapping f as follows:

$$\hat{X}^P = f(X_h; G; \Theta), \quad (1)$$

where \hat{X}^P is the prediction of future traffic data, and Θ is the set of all trainable parameters of f .

4. Methodology

Fig. 2 illustrates the overall architecture of STEI-PCN, which is composed of four parts: joint spatial-temporal relationship construction, local synchronous joint spatial-temporal correlations modeling, long-range temporal correlations modeling, and multi-view collaborative predicting. In the following, we delve into the details of each component.

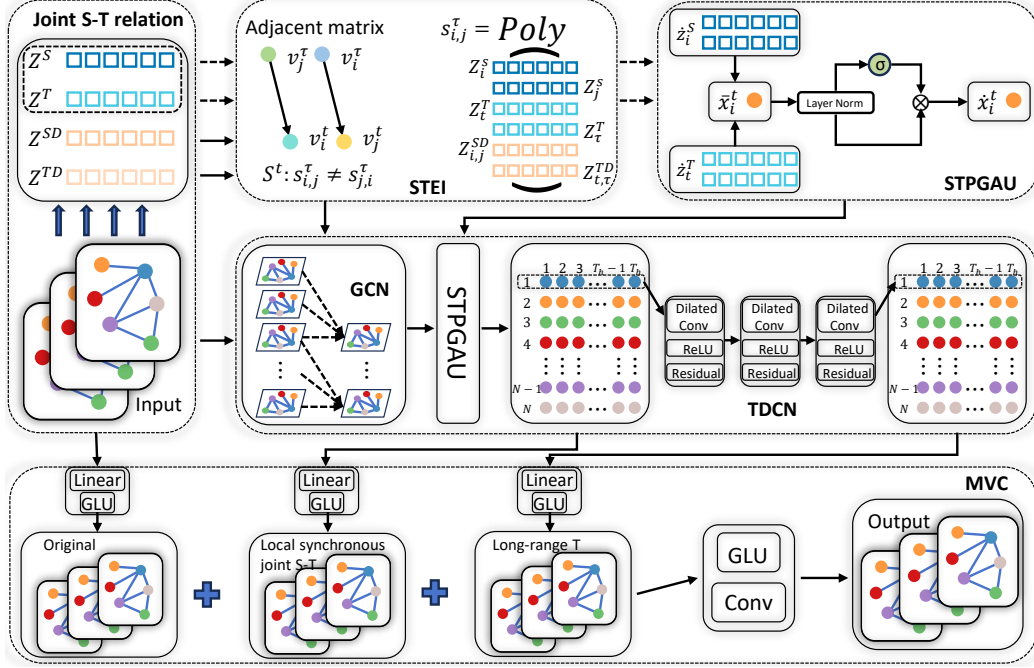


Figure 2: Illustration of STEI-PCN. After encoding the absolute and relative spatial and temporal information of nodes, the dynamic synchronous joint spatial-temporal weight matrix is learned using the polynomial-based inference module STEI. GCN extracts local synchronous joint spatial-temporal features, and STPGAU fuses local spatial and temporal information into node features to generate specific pattern features. Long-range temporal dependencies are captured using three layers of TDCN. Finally, original, local synchronous joint spatial-temporal, and long-range temporal features are processed through linear layers and GLU and concatenated. This concatenated data is then processed again with GLU and adjusted via two-dimensional convolutional layer to predict traffic data.

4.1. Joint spatial-temporal relation constructing

4.1.1. Joint spatial-temporal graph

We employ a GCN-based approach to achieve local synchronous joint spatial-temporal correlations modeling, where constructing a spatial-temporal graph that represents local joint spatial-temporal relationships is the core issue. Inspired by the spatial-temporal propagation characteristics exhibited by the evolution of node states in traffic networks, we introduce the spatial-temporal graph A_{STP} [19]. It can synchronously model the local joint spatial-temporal correlations between nodes, thereby more accurately capturing the local dynamic evolution patterns of node states in traffic networks.

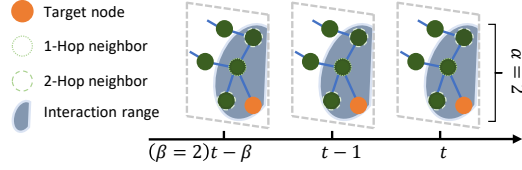


Figure 3: Illustration of the spatial-temporal interaction range. The shaded area indicates the interaction range where the target node can capture the spatial-temporal influences. The interaction range is determined by two hyper-parameters (α, β) , where α and β denote the maximum spatial hopping distance and the maximum temporal distance that the target node can access, respectively [19].

As shown in Fig. 3 [19], the target node at timestamp t is connected to the historical timestamps of local neighbor nodes within a specified range. Hyperparameters (α, β) are used to specify the interaction range between the target node and its spatial-temporal neighbors, simulating the characteristic of gradually decaying influence strength. The adjacency matrix representation of A_{STP} is as follows:

$$A_{STP}^t = \begin{matrix} & t & t-1 & \dots & t-\beta \\ t & A & A & \dots & A \end{matrix} \cdot \quad (2)$$

All spatial-temporal edges in $A_{STP}^t \in \mathbb{R}^{N \times (\beta+1)N}$ are unidirectionally connected to ensure temporal causality. $A \in \mathbb{R}^{N \times N}$ represents the α -hop adjacency matrix of the traffic network, formally defined as follows:

$$A_{ij} = \begin{cases} 1 & \text{if } SDist(v_i, v_j) \leq \alpha, \\ 0 & \text{otherwise,} \end{cases} \quad (3)$$

where $SDist(v_i, v_j)$ is the length of the shortest spatial path between nodes v_i and v_j in the spatial-temporal graph.

4.1.2. Spatial-temporal encoding

The accuracy of GCN in capturing local synchronous joint spatial-temporal features highly depends on the adjacency matrix used in the information aggregation process. Temporal and spatial coordinates and distances are the most intuitive and critical factors influencing local synchronous joint spatial-temporal correlations. Inspired by the inference component STPRI [19], we systematically encode these factors and integrate them into the subsequent inference process of the adjacency matrix, thereby further optimizing the

spatial-temporal coupling mechanism and enhancing the model’s ability to model complex spatial-temporal relationships.

1) *Spatial and Temporal Absolute-Coordinate Encoding*: Absolute spatial coordinates refer to the labels of nodes in the spatial dimension. In a traffic network, given all nodes $V = \{v_1, v_2, \dots, v_N\}$ and their unique spatial labels $i \in \{1, 2, \dots, N\}$, a trainable encoding vector $z_i^S \in \mathbb{R}^d$ is generated for each spatial label i .

Absolute temporal coordinates refer to the labels of nodes in the temporal dimension. Given all timestamps $t \in \{1, 2, \dots, T\}$ and their unique temporal labels $m \in \{1, 2, \dots, T_d\}$ and $n \in \{1, 2, \dots, 7\}$, two trainable encoding vectors $z_m^D \in \mathbb{R}^d$ and $z_n^W \in \mathbb{R}^d$ are generated for each timestamp t . Here, T_d represents the number of timestamps recorded by a sensor within a day, and 7 denotes the number of days in a week. For each timestamp t , z_m^D and z_n^W are combined to obtain the final encoding vector:

$$z_t^T = z_m^D + z_n^W. \quad (4)$$

2) *Spatial and Temporal Relative-Distance Encoding*: Relative spatial distance refers to the length of the shortest path between nodes in the spatial dimension of the spatial-temporal graph. When constructing the spatial-temporal graph, the maximum spatial interaction distance α between nodes and their unique spatial distance label $a \in \{0, 1, 2, \dots, \alpha\}$ are specified. A trainable encoding vector $z_a^{SD} \in \mathbb{R}^d$ is generated for each spatial distance a .

Relative temporal distance refers to the length of the shortest path between nodes in the temporal dimension of the spatial-temporal graph. When constructing the spatial-temporal graph, the maximum temporal interaction distance β between nodes and their unique temporal distance label $b \in \{0, 1, 2, \dots, \beta\}$ are specified. A trainable encoding vector $z_b^{TD} \in \mathbb{R}^d$ is generated for each temporal distance b .

4.2. Localized synchronous joint spatial-temporal correlations modeling

4.2.1. Spatial-temporal encode inferring

We design a spatial-temporal encode inferring (STEI) component based on polynomial functions, utilizing the aforementioned four types of spatial and temporal encodings to infer the dynamic joint spatial-temporal interaction strength between nodes.

The core idea of the inference component is to learn six polynomial functions $poly(\cdot)$, which can map the four types of six encoding vectors associated with the nodes to corresponding dynamic weights. This process aims

to more precisely and meticulously characterize the dynamic joint spatial-temporal interaction strength and characteristics between nodes, thereby enhancing the model’s interpretability and its ability to capture complex spatial-temporal patterns. Given the target node v_i^t at timestamp t and its neighbor nodes v_j^τ within the interaction range (α, β) , where $i, j \in \{1, 2, \dots, N\}$, $\tau \in \{t - \beta, t - \beta + 1, \dots, t\}$. We use $\mathbf{S}^t = \{s_{i,j}^\tau | i, j = 1, 2, \dots, N; \tau = t - \beta, t - \beta + 1, \dots, t\} \in R^{N \times (\beta+1)N}$ to represent the dynamic weights of all spatial-temporal edges within the interaction range at time t , and update the adjacency matrix:

$$A_{STP}^t = \mathbf{S}^t, \quad (5)$$

where each element is defined as follows:

$$s_{ij}^\tau = \begin{cases} \exp(\text{poly}_1(z_i^S)) + \exp(\text{poly}_2(z_j^S)) \\ + \exp(\text{poly}_3(z_t^T)) + \exp(\text{poly}_4(z_\tau^T)) \\ + \exp(\text{poly}_5(z_{\text{SDist}(v_i, v_j)}^{SD})) \\ + \exp(\text{poly}_6(z_{\text{TDist}(t, \tau)}^{TD})) & \text{if } \text{SDist}(v_i^t, v_j^\tau) \leq \alpha, \\ 0 & \text{otherwise,} \end{cases} \quad (6)$$

where z_i^S, z_j^S represent the absolute spatial coordinate encoding vectors of nodes v_i^t, v_j^τ respectively, z_t^T, z_τ^T represent the absolute temporal coordinate encoding vectors of timestamps t, τ respectively, and $z_{\text{SDist}(i, j)}^{SD}, z_{\text{TDist}(t, \tau)}^{TD}$ represent the encoding vectors of the relative spatial distance $\text{SDist}(v_i, v_j)$ and the relative temporal distance $\text{TDist}(t, \tau)$ between nodes respectively. The polynomial functions $\text{poly}_k(\cdot)$ are learnable and defined as follows:

$$\text{poly}_k(z_i^S) = -\|z_i^S - \mu_k\|, \quad (7)$$

where $\mu_k \in R^d$ is a trainable parameter vector, $\|\cdot\|$ denotes the euclidean norm, and the $\exp(\cdot)$ function is used to map the inference results of the polynomial functions to the interval $[0, 1]$. Moreover, this inference component can use spatial-temporal prior information to initialize the adjacency matrix A_{STP}^t to obtain a prior local joint spatial-temporal weight matrix. Therefore, STEI is not only easier to train but also more effective in reducing the risk of overfitting.

It is noteworthy that the total number of parameters in STEI is $6d$, compared to the total number of parameters in STPRI $12d$ [19], the number

of parameters is halved, and the computational complexity is reduced from $O(d^2)$ to $O(d)$, which is also one of the main reasons for the significant improvement in the computational efficiency of our model.

4.2.2. Localized synchronous joint spatial-temporal graph convolution

We further utilize the inferred dynamic adjacency matrix A_{STP}^t , combined with a single-layer GCN incorporating the gated activation unit STPGAU [19] that includes absolute temporal and spatial coordinates information, to capture local synchronous joint spatial-temporal dependencies. The GCN operation consists of two steps: aggregation and update of node features, and gated activation of node features integrating absolute temporal and spatial coordinates information.

1) *Aggregation and update of nodes features*: Using the inferred dynamic adjacency matrix A_{STP}^t , we construct the following aggregation function:

$$\tilde{X}_i^H = \mathbf{A}_{STP}^t X_i^H = \mathbf{S}^t \mathbf{X}_i^H, \quad (8)$$

where $\mathbf{X}_i^H = [\mathbf{X}_{t-\beta}^H, \dots, \mathbf{X}_t^H]^\top \in \mathbb{R}^{N \times (\beta+1)N \times C}$ represents the node feature matrix composed of $\beta + 1$ time steps. If the timestamp $\tau \in \{t - \beta, t - \beta + 1, \dots, t\}$ exceeds the input time series, the original feature data at that moment is filled with a zero matrix.

Each element is defined as follows:

$$\tilde{x}_i^t = \sum_{j=1}^N \sum_{\tau=t-\beta}^t s_{ij}^\tau x_j^\tau, \quad (9)$$

where $s_{i,j}^\tau$ denotes the dynamic weight of the spatial-temporal edge between nodes v_i^t and v_j^τ , and $x_j^\tau \in R^C$ represents the encoded data of node v_j at timestamp τ . We use a linear layer to initialize the encoding of the original traffic data (flow or speed) to obtain $x_j^\tau = \mathbf{W}^0 \cdot \mathbf{x}_j^\tau + \mathbf{b}^0$, where $\mathbf{x}_j^\tau \in X$ is the original traffic feature data, and the linear layer weights $W^0 \in R^{C \times 1}$ and bias $b^0 \in R^C$ are trainable parameters.

According to equation (9), node features at different timestamps are dynamically aggregated onto the target node v_i^t . Next, we increase the dimensions of the node features to $2C$ through linear transformation to enhance the model's linear representation capability, with the update formula as follows:

$$\bar{x}_i^t = \mathbf{W}^1 \cdot \tilde{x}_i^t + \mathbf{b}^1, \quad (10)$$

where the linear layer weights $W^0 \in R^{C \times 1}$ and bias $b^0 \in R^C$ are trainable parameters.

2) *Nodes Features Gating Activation*: GCN update the feature of target node by aggregating features from neighboring nodes. After integrating a large amount of data, maintaining the uniqueness of nodes features becomes relatively challenging. Previous techniques typically achieve the integration of feature data with temporal and spatial information by encoding temporal and spatial features during the initial encoding stage of traffic data, and concatenating these with the encoded node features. In contrast, the introduced STPGAU achieves the fusion of temporal and spatial information with the results of GCN, aiding in remembering the unique patterns of node features. Specifically, within the STPGAU, absolute temporal and spatial coordinate encodings are used as guiding information. GLU is introduced to scale the fused results, thereby learning the unique patterns of nodes. This process is detailed as follows:

$$\begin{aligned} \dot{x}_i^t &= (\mathbf{W}^4 \cdot (\bar{x}_i^t + \mathbf{W}^2 \cdot \dot{z}_i^S + \mathbf{b}^2 + \mathbf{W}^3 \cdot \dot{z}_i^T + \mathbf{b}^3) + \mathbf{b}^4) \\ &\otimes \delta(\mathbf{W}^5 \cdot (\bar{x}_i^t + \mathbf{W}^2 \cdot \dot{z}_i^S + \mathbf{b}^2 + \mathbf{W}^3 \cdot \dot{z}_i^T + \mathbf{b}^3) + \mathbf{b}^5), \end{aligned} \quad (11)$$

where \otimes denotes element-wise multiplication, δ represents the sigmoid activation function, and the linear layer weights $\mathbf{W}^2, \mathbf{W}^3$, convolutional kernels $\mathbf{W}^4, \mathbf{W}^5$, and biases $\mathbf{b}^2, \mathbf{b}^3, \mathbf{b}^4, \mathbf{b}^5$ are trainable parameters. The encoded absolute spatial coordinate \dot{z}_i^S is used to characterize the spatial feature of node v_i^t , while the encoded absolute temporal coordinate \dot{z}_i^T is used to characterize the features of timestamp t . The local absolute temporal and spatial information is integrated into the updated node features and added as guiding information to the GLU, enabling the GLU to perceive the individual characteristics of the nodes and adjust the output, thereby generating node-specific features.

4.3. Long-range temporal correlations modeling

In many tasks, the TDCN offers superior performance compared to RNN, while avoiding common pitfalls of recursive models such as gradient explosion, gradient disappearance, or inadequate memory retention. We employ three layers of TDCN to capture long-range temporal dependencies.

Let $\dot{\mathbf{X}}_i = [\dot{x}_i^1, \dot{x}_i^2, \dots, \dot{x}_i^{T_h}]$ denotes the output sequence of length T_h for node v_i after local synchronous joint spatial-temporal feature extraction. Also, let $\dot{\mathbf{X}}_i^l = [\dot{x}_i^{1,l}, \dot{x}_i^{2,l}, \dots, \dot{x}_i^{T_h,l}]$ represent the output sequence of node

v_i after processing through the $(l - 1)$ th layer of TDCN, which serves as the input to the l th layer.

For a set of trainable parameters $\{w_i^{t-(k-1)d,l}, w_i^{t-(k-2)d,l}, \dots, w_i^{t,l}\}$, where d is the dilation factor and k is the size of the dilated convolution kernel, we define the dilated causal convolution operation on the historical input sequence at timestamp $t \in \{1, 2, \dots, T_h\}$ in the l th layer as follows:

$$\dot{x}_i^{t,l+1} = \text{ReLU}\left(\sum_{r=1}^k w_i^{t-(r-1)d,l} \cdot x_i^{t-(r-1)d,l}\right). \quad (12)$$

To accelerate the training process of the model and improve its convergence performance, residual connection mechanism is introduced in each layer of the TDCN. Overall, we stack three layers of TDCN with fixed convolutional kernel size of 3×1 , with dilation factors sequentially specified as 1, 2, and 4, corresponding padding amounts of 1, 2, and 4, and channel counts of C , $2C$, and $4C$, respectively, all employing the ReLU activation function, and each layer features use residual connections. Through this design, the network’s effective receptive field grows exponentially, thus being able to comprehensively cover all historical outputs for any given timestamp t . This enables the model to efficiently capture long-range causal temporal dependencies within the network. Additionally, to maintain consistency in the number of output feature channels, a two-dimensional convolutional layer is added at the end to adjust the number of output channels. Fig. 4 illustrates a schematic diagram of stacking these three layers of TDCN.

4.4. Multi-view collaborative predicting

4.4.1. Skip connections with GLU

The GLU is a relatively simple gating mechanism that includes only one output gate. We use GLU to control the output of feature data from each perspective. Let $X^i = [\chi_1^i, \chi_2^i, \dots, \chi_N^i] \in R^{T_h \times N \times C}$, where χ_k^i represents the feature data of duration T_h obtained by node v_k in the i -th perspective. First, the dimension of X^i is compressed through a two-dimensional convolutional layer to reduce memory consumption:

$$\tilde{X}^i = \mathbf{W}^6 \cdot X^i + \mathbf{b}^6, \quad (13)$$

where the convolution kernel \mathbf{W}^6 and bias \mathbf{b}^6 are trainable parameters, and $\tilde{X}^i \in R^{C \times N \times 1}$. The gating activation of GLU can be expressed as:

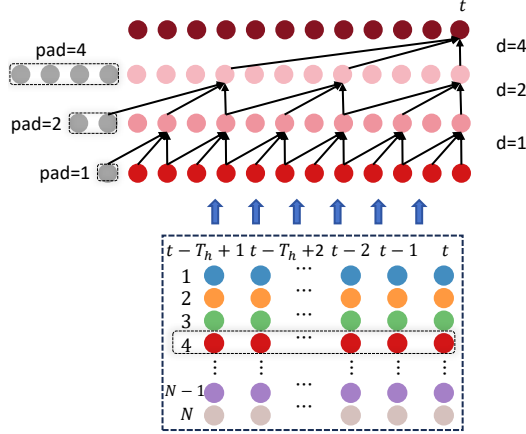


Figure 4: Overall structure of stacking three layers of TDCN.

$$\bar{X}^i = (\mathbf{W}^7 \cdot \tilde{X}^i + \mathbf{b}^7) \otimes \delta(\mathbf{W}^8 \cdot \tilde{X}^i + \mathbf{b}^8), \quad (14)$$

where \otimes denotes element-wise multiplication, δ represents the sigmoid activation function, and the convolution kernels $\mathbf{W}^7, \mathbf{W}^8$ and biases $\mathbf{b}^7, \mathbf{b}^8$ are trainable parameters.

4.4.2. Multi-view prediction layer

Through skip connections, we concatenate the feature data from three perspectives to obtain $\bar{X} = \bar{X}^1 || \bar{X}^2 || \bar{X}^3$, where $||$ denotes the concatenation operation. Again, we use GLU to process $\bar{X} \in R^{3C \times N \times 1}$ to get \dot{X} in order to enhance the capability of nonlinear expression. The result is then fed into a two-dimensional convolutional layer to encode the features of all nodes over the time dimension, generating future predictions $\hat{X}^p \in R^{T_p \times N \times 1}$, where T_p is the prediction time steps. Unlike early models that recursively generate the prediction sequence requiring T_p steps, our model outputs the prediction sequence of length T_p in one go. Additionally, by setting different values for T_p , we can predict traffic data for any number of time steps into the future.

4.5. Model training and analyzing

4.5.1. Loss function

The model is trained using the Mean Absolute Error (MAE) loss function. Assuming Θ represents all trainable parameters in STEI-PCN, the objective function is defined as follows:

$$\arg \min_{\Theta} \sum_{t=1}^{T_p} \sum_{i=1}^N |\hat{X}^P(t, i) - X^P(t, i)|, \quad (15)$$

where \hat{X}^P denotes the predicted results, while X^P represents the true features.

4.5.2. Model complexity calculating

To construct a joint spatial-temporal relationship, it is necessary to first search the adjacency matrix $A_{STP}^t \in R^{N \times (\beta+1)N}$. The computational complexity of the search operation is $O(\alpha NQ)$, where N is the total number of nodes, and Q (typically much smaller than N) represents the maximum number of α -hop neighbors for all nodes. When generating the encoding vectors, since the aforementioned search process has already recorded the relative temporal and spatial distance information between nodes, the computational complexity of this operation is only $O(1)$. In the STEI component, the computational complexity of the polynomial function is $O(d)$. M (typically much smaller than $(\beta + 1)N^2$) denotes the total number of connected spatial-temporal edges $s_{i,j}^{\tau}$, and the computational complexity of the inference component is $O(dT_hM)$. In the GCN, the computational complexities of the aggregation and update operations are $O(T_hMC)$ and $O(T_hNC^2)$, respectively. The computational complexity of the STPGAU component is $O(T_hNC^2 + dT_hNC)$ [19]. The total computational complexity of three layers of TDCN is $O(T_hNCC_1 + T_hNC_1C_2 + T_hNC_2C_3)$, and the computational complexity of the convolutional layer used to adjust the number of channels is $O(T_hNC_3C)$, where $C_1 = C, C_2 = 2C, C_3 = 4C$ are the output channel numbers of the three layers of TDCN, respectively. Therefore, the computational complexity of the entire long-range temporal correlations module is $O(T_hNC^2)$. The computational complexity of the MVC module using GLU is also $O(T_hNC^2)$.

In summary, the total computational complexity of the entire model is $O(\alpha NQ + dT_hM + T_hMC + T_hNC^2 + dT_hNC)$.

5. Experiment

5.1. Datasets

To assess the performance of STEI-PCN, we conduct comprehensive multi-scenario experiments using four traffic flow datasets (PeMS03/04/07/08 [15]),

Dataset	Nodes	Time steps(5min)	Time range	Missing ratio	Type
PeMS03	358	26208	09/2018-11/2018	0.672%	Flow
PeMS04	307	16992	01/2018-02/2018	3.182%	Flow
PeMS07	883	28224	05/2017-08/2017	0.452%	Flow
PeMS08	170	17856	07/2016-08/2016	0.696%	Flow
PeMS-Bay	325	52116	01/2017-05/2017	0.003%	Speed

Table 1: Details of datasets.

as well as a traffic speed dataset (PeMS-Bay [12]). Detailed information is provided in Table 1. These diverse datasets encompass a wide range of traffic environments and offer a rich variety of testing scenarios, enabling a thorough and in-depth evaluation of the model’s performance in the field of traffic.

5.2. Experiment settings

The experiments are conducted on a server equipped with an NVIDIA RTX 4090 GPU (24GB memory), a 16-core Intel(R) Xeon(R) Gold 6430 CPU, and 120GB of RAM. We utilize data from $T_h = 12$ consecutive time steps as input to predict the data for the next T_p time steps, where T_p is specified to be in the range of (3, 6, 12). The model is validated on the validation set using an early stopping strategy. The process is repeated five times with different random seeds, and the model that performs best on the validation set is selected as the final model for evaluation, with the average taken as the evaluation metric. The Adam optimizer is used during training, with the learning rate set to 0.002. The hyperparameters of the model are configured as follows: $\alpha = 4$, $\beta = 2$, $d = 6$, $C = 64$, $kernel\ size = 3$, $dilation = (1, 2, 4)$. For the PeMS03 and PeMS-Bay datasets, the number of training epochs is set to 60, with a batch size of 32. For the PeMS04, PeMS07, and PeMS08 datasets, the number of training epochs is set to 200, with batch sizes of 32 and 18 (due to the large size of the PeMS07 dataset, the maximum batch size can only be set to 18). Consistent with the benchmarks in previous studies, the PeMS-Bay dataset is divided into training, validation, and test sets in a ratio of 7 : 1 : 2 [12], while the other datasets are divided in a ratio of 6 : 2 : 2 [15].

5.3. Evaluation metrics

All tasks are evaluated using three widely-adopted evaluation metrics: MAE, RMSE and MAPE. The definitions of these metrics are as follows:

$$\text{MAE} = \frac{1}{N} \sum_{i=1}^N |\hat{x}_i^p - x_i^p|, \quad (16)$$

$$\text{RMSE} = \sqrt{\frac{1}{N} \sum_{i=1}^N (\hat{x}_i^p - x_i^p)^2}, \quad (17)$$

$$\text{MAPE} = \frac{100\%}{N} \sum_{i=1}^N \left| \frac{\hat{x}_i^p - x_i^p}{x_i^p} \right|, \quad (18)$$

where x_i^p , \hat{x}_i^p is the actual flow and the predicted flow, respectively. N is the total number of nodes.

5.4. Baseline models

To evaluate STEI-PCN, it is compared with the following baseline models. Models based on a decoupled architecture that separately extract temporal and spatial correlations: DCRNN [12]; STGCN [13]; ASTGCN [29]; GWN [14]; AGCRN [31]; GMAN [23]; MTGNN [30]; STNorm [15]; Z-GCNETs [34]; DSTAGNN [32]; STEP [37]; STID [39]; DGCRN [33]; PDFormer [24]; STAEformer [40]; STD-MAE [38]; STWave [44]; HTVGNN [35]; RGDAN [27]; DTRformer [41]. Models that employ a joint module to synchronously extract temporal and spatial correlations: STSGCN [15], STFGCN [16], T-Graphormer [17]. Model based on a decoupled architecture that separately extract temporal, spatial, and spatial-temporal correlations: SSGCRTN [21]. Model that utilizes a joint module to synchronously extract temporal, spatial, and spatial-temporal correlations: STPGCN [19].

5.5. Experiment results

Table 2 presents the experiment results of STEI-PCN and baseline models on traffic flow datasets for a prediction horizon of half an hour (horizon=6), while Table 3 provides the results of STEI-PCN and baseline models on traffic speed dataset for prediction horizons of 15 minutes (horizon=3), half an hour (horizon=6), and one hour (horizon=12). The following conclusions can be drawn:

(i) Static graph models exhibit significant variability in performance for traffic prediction tasks. Models based on GCN combined with RNN/TCN (DCRNN [12], STGCN [13], and GMAN [23]) show relatively poor performance. In contrast, static graph models using embedding mechanisms and

Model	PEMS03			PEMS04			PEMS07			PEMS08		
	MAE	RMSE	MAPE	MAE	RMSE	MAPE	MAE	RMSE	MAPE	MAE	RMSE	MAPE
DCRNN(2017)	15.54	27.18	15.62%	19.63	31.26	13.59%	21.16	34.14	9.02%	15.22	24.17	10.21%
STGCN(2017)	15.83	27.51	16.13%	19.57	31.38	13.44%	21.74	35.27	9.24%	16.08	25.39	10.60%
ASTGCN(2019)	17.69	29.66	19.40%	22.93	35.22	16.56%	28.05	42.57	13.92%	18.61	28.16	13.08%
GWN(2019)	14.59	25.24	15.52%	18.53	29.92	12.89%	20.47	33.47	8.61%	14.40	23.39	9.21%
AGCRN(2020)	15.24	26.65	15.89%	19.38	31.25	13.40%	20.57	34.40	8.74%	15.32	24.41	10.03%
GMAN (2020)	16.87	27.92	18.23%	19.14	31.60	13.19%	20.97	34.10	9.05%	15.31	24.92	10.13%
MTGNN(2020)	14.85	25.23	14.55%	19.17	31.70	13.37%	20.89	34.06	9.00%	15.18	24.24	10.20%
STSGCN (2020)	17.48	29.21	16.78%	21.19	33.65	13.90%	24.26	39.03	10.21%	17.13	26.80	10.96%
STNorm(2021)	15.32	25.93	14.37%	18.96	30.98	12.69%	20.50	34.66	8.75%	15.41	24.77	9.76%
Z-GCNETs (2021)	16.64	28.15	16.39%	19.50	31.61	12.78%	21.77	35.17	9.25%	15.76	25.11	10.01%
DSTAGNN (2022)	15.57	27.21	14.68%	19.30	31.46	12.70%	21.42	34.51	9.01%	15.67	24.77	9.94%
STEP(2022)	14.22	24.55	14.42%	18.20	29.71	12.48%	19.32	32.19	8.12%	14.00	23.41	9.50%
STFGCN(2022)	16.77	28.34	16.30%	19.83	31.88	13.02%	22.07	35.80	9.21%	16.64	26.22	10.60%
STID(2022)	15.33	27.40	16.40%	18.29	29.86	12.46%	19.59	32.90	8.30%	14.21	23.57	9.24%
STPGCN(2022)	14.99	24.83	14.97%	18.46	30.15	12.01%	19.70	32.99	8.19%	13.81	23.58	9.06%
DGCRN(2023)	14.60	26.20	14.87%	18.84	30.48	12.92%	20.04	32.86	8.63%	14.77	23.81	9.77%
PDFormer(2023)	14.94	25.39	15.82%	18.32	29.97	12.10%	19.83	32.87	8.53%	13.58	23.51	9.05%
STAEformer(2023)	15.35	27.55	15.18%	18.22	30.18	11.98%	19.14	32.60	8.01%	13.46	23.25	8.88%
STWave(2023)	14.92	26.70	15.53%	18.68	30.62	12.62%	19.48	33.32	8.16%	13.69	23.47	9.40%
STD-MAE(2023)	<u>13.80</u>	<u>24.43</u>	13.96%	17.80	<u>29.25</u>	11.97%	<u>18.65</u>	<u>31.44</u>	<u>7.84%</u>	13.44	<u>22.47</u>	8.76%
HTVGNN(2024)	14.30	24.59	14.69%	18.01	29.81	<u>11.89%</u>	19.50	32.65	8.15%	13.28	22.83	<u>8.65%</u>
SSGCRTN(2024)	15.18	26.52	14.66%	19.28	31.17	12.68%	20.71	34.22	8.69%	15.18	24.32	9.59%
DTRformer(2025)	14.50	25.45	14.94%	<u>18.00</u>	29.58	12.30%	18.99	32.23	7.93%	<u>13.17</u>	22.85	8.66%
STEI-PCN(ours)	13.78	22.17	<u>14.26%</u>	17.80	29.16	11.74%	18.33	30.66	7.67%	13.03	21.87	8.50%

Bold: best, underline: second best

Table 2: Performance comparison with different baseline models on the PeMS03/04/07/08 datasets.

attention mechanisms (PDFformer [24] and RGDAN [27]) demonstrate superior performance. This indicates that attention mechanisms have a significant advantage in extracting temporal and spatial features, as their adaptive weight allocation mechanisms effectively enhance the model’s representational capabilities.

Moreover, dynamic graph models exhibit stronger modeling capabilities in capturing temporal and spatial correlations. Dynamic graph models such as MTGNN [30], DSTAGNN [32], and DGCRN [33] achieve significant performance improvements by capturing dynamic temporal and spatial correlations. Among them, HTVGNN [35], as a competitive baseline model, combines GCN with attention mechanisms to effectively extract temporal and spatial features, achieving suboptimal results on some metrics. This further validates the advanced and effective nature of attention mechanisms in traffic prediction tasks.

In terms of synchronous temporal and spatial modeling, STSGCN [15] and STFGNN [16] capture temporal and spatial correlations synchronously, aligning more closely with the actual evolution of traffic states. However, these models’ heavy reliance on GCN architectures significantly increases

Model	Horizon 3			Horizon 6			Horizon 12		
	MAE	RMSE	MAPE	MAE	RMSE	MAPE	MAE	RMSE	MAPE
STEP (2022)	1.26	2.73	2.59%	1.55	3.58	3.43%	1.79	<u>4.20</u>	4.18%
STID (2022)	1.30	2.81	2.73%	1.62	3.72	3.68%	1.89	4.40	4.47%
PDFormer (2023)	1.32	2.83	2.78%	1.64	3.79	3.71%	1.91	4.43	4.51%
STAEformer (2023)	1.31	2.78	2.76%	1.62	3.68	3.62%	1.88	4.34	4.41%
STD-MAE (2023)	<u>1.23</u>	2.62	<u>2.56%</u>	1.53	3.53	3.42%	<u>1.77</u>	<u>4.20</u>	<u>4.17%</u>
RGDAN (2024)	1.31	2.79	2.77%	1.56	3.55	3.47%	1.82	<u>4.20</u>	4.28%
T-Graphormer (2025)	1.31	<u>2.55</u>	2.71%	<u>1.52</u>	3.14	<u>3.23%</u>	1.76	3.78	3.91%
STEI-PCN (ours)	1.17	2.46	2.33%	1.47	<u>3.35</u>	3.12%	1.88	4.42	4.28%

Bold: best, underline: second best

Table 3: Performance comparison with different baseline models on the PeMS-Bay dataset.

the number of parameters, leading to higher training and inference time and slower convergence rates. Experimental results show that on most benchmark datasets, models with decoupled architectures (*e.g.*, DSTAGNN, DGCRN, etc.) outperform STSGCN and STFGNN, indicating that there is still considerable room for optimization in synchronous temporal and spatial modeling architectures. The recently proposed T-Graphormer [17] validates this point, achieving significant performance improvements on the PeMS-Bay speed dataset and obtaining optimal or suboptimal results on most evaluation metrics, providing a new direction for future research.

(ii) Among non-graph-structured prediction models, transformer-based architectures demonstrate significant advantages. Models such as STEP [37], STAEformer [40], and DTRformer [41] achieve excellent performance in experimental results, with DTRformer reaching suboptimal results on some metrics. This not only further validates the advanced and effective nature of attention mechanisms in traffic prediction tasks but also reflects the trend of research in traffic prediction moving toward transformer-based architectures. Notably, the STD-MAE [38], which employs an encoder-decoder structure, performs particularly well, achieving optimal or suboptimal results on the majority of evaluation metrics, establishing its position as a highly competitive baseline model in the field. This may provide new references for the design and optimization of future traffic prediction models.

(iii) Models using joint spatial-temporal correlations architectures (SS-GCRTN [21] and STPGCN [19]) theoretically have stronger modeling capabilities compared to models that only combine temporal and spatial correlations. In particular, STPGCN’s design of a synchronous joint spatial-temporal correlations architecture aligns more closely with the evolution

patterns of node states in traffic networks, enabling more accurate capture of nonlinear dynamic evolution features. Its performance surpasses these of contemporaneous and earlier models. However, compared to subsequently proposed models that only combine temporal and spatial correlations, STPGCN’s performance still shows a noticeable gap. This indicates that there is still significant potential for optimization and innovation in this architecture.

Guided by this idea, we further improve the joint spatial-temporal correlations architecture, using a local synchronous joint spatial-temporal correlations combined with long-range temporal correlations architecture to build our model for better performance. It can be seen that STEI-PCN almost comprehensively outperforms the aforementioned baseline models on all traffic flow datasets and achieves near-comprehensive superiority over the baseline models in medium-term prediction tasks on the speed dataset.

Fig. 5 shows the comparison of metrics between STEI-PCN and some representative advanced baseline models on four traffic flow datasets for prediction horizons $T_h = 3, 6, 12$. From the figure, it can be observed that as T_h increases, prediction complexity also rises, leading to gradual increases in evaluation metrics MAE, RMSE, and MAPE. Further analysis reveals that for short-term predictions, our model demonstrates the best performance across all datasets. However, in long-term prediction tasks, model performance shows some variability: It performs relatively poorly on the PeMS-Bay dataset but maintains optimal performance on the traffic flow datasets. We speculate that this phenomenon may be related to the more frequent and intensive mutation characteristics in the speed dataset, where STEI-PCN exhibits certain limitations in handling such dataset with multiple mutations. Nevertheless, the overall experimental results allow us to conclude that the STEI-PCN demonstrates good applicability in any term prediction tasks, with particularly outstanding performance in short-term prediction tasks, validating the model’s universality and robustness when applied to traffic prediction tasks of different durations.

The outstanding performance of STEI-PCN across datasets can be attributed to three main factors: (i) The model considers local synchronous joint spatial-temporal correlations, which align closely with the graph structure characteristics of road networks and the evolution patterns of traffic flow and speed within such networks. By explicitly capturing long-range causal temporal correlations, the model enhances its understanding of temporal context. (ii) Through systematic hyperparameter grid search, we identify

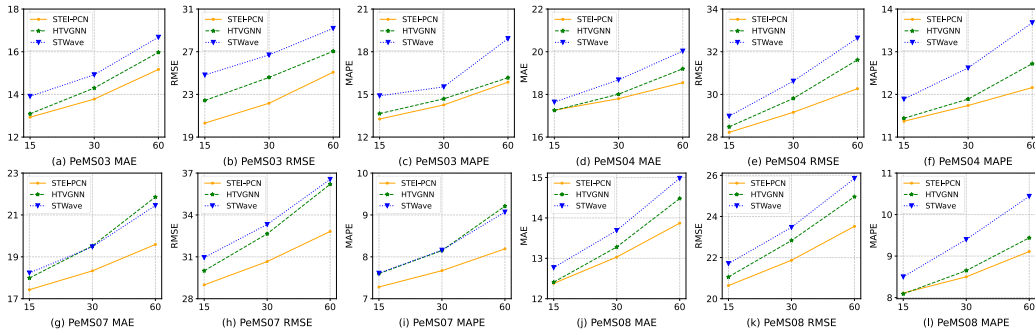


Figure 5: Comparison of models performance for three horizons on the PeMS03/04/07/08 datasets.

optimal parameters influencing the three correlations, achieving an optimal balance between local and global feature extraction for these correlations. (iii) The model integrates features data from three different perspectives, enabling more comprehensive evaluation and prediction. These characteristics collectively ensure the efficiency, accuracy, and stability of STEI-PCN across multiple dataset prediction tasks and different prediction horizons.

Fig. 6 shows the comparison for prediction horizons of an hour (horizon=12) between STEI-PCN’s predictions and ground truth values for four randomly selected nodes over one day (288 timestamps) on the PeMS03 and PeMS-Bay datasets. For the speed dataset PeMS-Bay, we zoom in on the comparison between predicted and actual values from 9:30 to 11:00, and for the traffic flow dataset PeMS03, we zoom in on the comparison from 5:30 to 7:00. It can be observed that even when traffic data undergoes abrupt changes, our model can still provide relatively accurate predictions. This result indicates that our model has the capability to capture mutation features in traffic data, demonstrating its superior performance in handling complex changes in traffic data.

5.6. Ablation study

To validate the effectiveness of each component of the model, we conduct ablation experiments for prediction horizons of an hour (horizon=12) using the PeMS04 and PeMS08 datasets and compare the convergence speed of STEI-PCN with two of its main variants. We designed nine variants as follows:

- w/o SCE Z^S : Removing the spatial absolute-coordinate encoding.

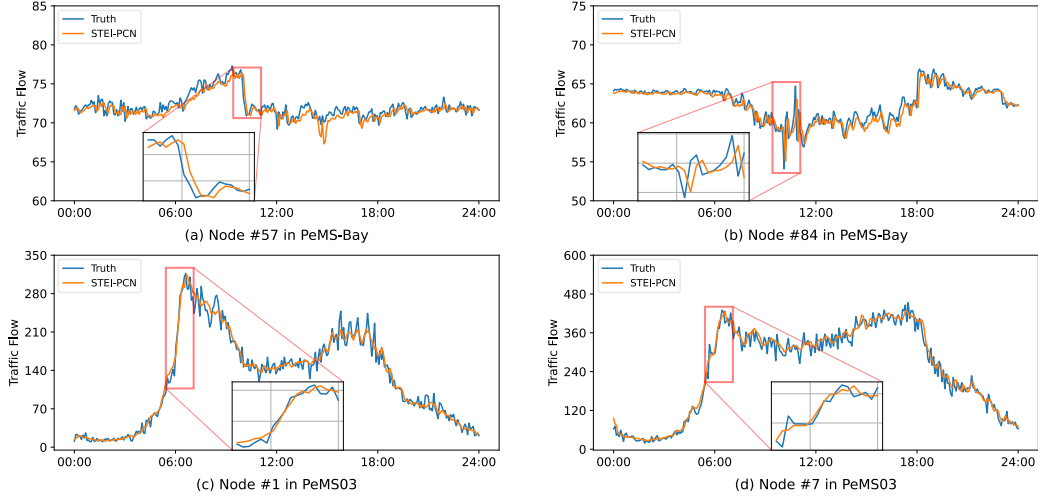


Figure 6: Visualization of prediction results on PeMS-Bay and PeMS03 datasets.

- w/o TCE \mathbf{Z}^T : Removing the temporal absolute-coordinate encoding.
- w/o SDE \mathbf{Z}^{SD} : Removing the spatial relative-distance encoding.
- w/o TDE \mathbf{Z}^{TD} : Removing the temporal relative-distance encoding.
- w/o STEI: Removing the spatial-temporal encode inferring module. The GCN is constructed using an adaptive joint spatial-temporal adjacency matrix.
- w/o STPGAU: Removing the spatial-temporal position-aware gated activation unit. In the initial feature encoding stage, temporal and spatial feature encoding is integrated to replace the STPGAU.
- w/o GCN: Removing the graph convolution networks.
- w/o TDCN: Removing the temporal dilated causal convolution module.
- w/o MVC: Remove the multi-view collaborative predicting module.

The experimental results, as shown in Table 4, lead to the following conclusions:

(i) The absence of any component leads to a decline in evaluation metrics, indicating that each component is necessary for the effectiveness and completeness of STEI-PCN.

Model	PeMS04			PeMS08		
	MAE	RMSE	MAPE	MAE	RMSE	MAPE
STEI-PCN	18.55	30.27	12.16%	13.87	23.52	9.11%
w/o SCE Z^S	20.75	33.32	14.04%	15.51	26.01	9.78%
w/o TCE Z^T	18.63	30.33	12.19%	13.89	23.60	9.16%
w/o SDE Z^{SD}	18.60	30.29	12.21%	13.91	23.67	9.13%
w/o TDE Z^{TD}	18.59	30.31	12.23%	13.90	23.62	9.14%
w/o STEI	18.95	30.73	12.45%	14.71	24.37	9.50%
w/o STPGAU (w/T & S)	19.45	31.44	12.78%	14.27	23.68	9.45%
w/o GCN	25.80	39.99	17.42%	20.83	32.26	13.00%
w/o TDCN	18.89	30.73	12.58%	14.46	23.88	9.34%
w/o MVC	24.50	40.60	16.22%	22.08	40.01	13.85%

w/o: without, w/: with

Table 4: Component analysis of the STEI-PCN on PeMS04/08 datasets.

(ii) The variants w/o SCE Z^S and w/o TCE Z^T exhibit poorer experimental results. This highlights the critical role of absolute spatial and temporal coordinate encodings in capturing local synchronous joint spatial-temporal correlations. Explicitly modeling absolute spatial and temporal coordinates enables the model to effectively maintain temporal and spatial contextual relationships among nodes, thereby enhancing its predictive performance. Additionally, the variants w/o SDE Z^{SD} and w/o TDE Z^{TD} show slightly worse results, further proving the beneficial impact of relative temporal and spatial distance modeling on prediction performance. This information helps explicitly describe the relative positional relationships between nodes.

(iii) STEI-PCN significantly outperforms the variant w/o STEI, demonstrating that a simple adaptive joint spatial-temporal adjacency matrix cannot effectively capture complex joint spatial-temporal relationships. In contrast, STEI efficiently captures these complex relationships and accurately assesses their importance.

(iv) The absence of either GCN or TDCN leads to a significant decline in performance, with the absence of GCN having a particularly pronounced impact. This phenomenon confirms the effectiveness of the architecture combining local synchronous joint spatial-temporal correlations with long-range temporal correlations, while also highlighting the criticality of local synchronous joint spatial-temporal correlations within this architecture.

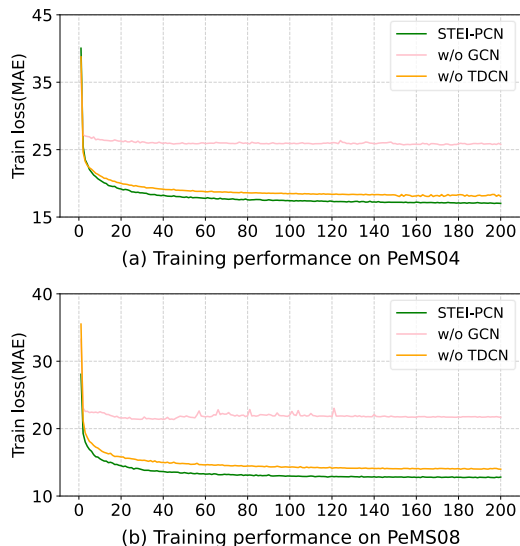


Figure 7: Comparison of training loss among STEI-PCN and its two main variants on the PeMS04/08 datasets.

(v) Removing STPGAU results in a decline in performance, proving the effectiveness of this gated unit in selecting key features and improving the model’s prediction accuracy.

(vi) The variant w/o MVC exhibits the worst experimental results, fully demonstrating the importance of the MVC module. By integrating feature data from three different perspectives, the model achieves more comprehensive evaluation and prediction, significantly enhancing overall performance.

Fig. 7 shows the convergence speed comparison of STEI-PCN with two main variants: w/o GCN and w/o TDCN on the training set. Notably, STEI-PCN not only significantly outperforms these two variants in evaluation metrics but also exhibits extremely fast convergence during training, reflecting the powerful learning capability of the architecture combining local synchronous joint spatial-temporal correlations with long-range temporal correlations.

5.7. Hyperparameter effects

STEI-PCN is based on a spatial-temporal graph, where two parameters specifying the spatial-temporal interaction range are crucial. The dimensions of the encoding vectors is also an important parameter, as it not only directly affects the quality of the encodings but also influences the expressive power of

the polynomial functions used for weight inference. Additionally, the number of TDCN in the long-range temporal correlations module is a key parameter, as it determines the effective receptive field which is the number of historical timestamps the model can cover during the capture of long-range temporal correlations. When adjusting one parameter, the other parameters are set to their default optimal values. Fig. 8 illustrates the performance of STEI-PCN for prediction horizons of an hour (horizon=12) on the PeMS-Bay dataset when varying four important hyperparameters, leading to the following conclusions: (i) As α and β increase, the model performance initially improves and then declines. This indicates that an appropriate spatial-temporal interaction range can balance the capture of local and global features, achieving a trade-off between prediction accuracy and robustness, which contributes to performance optimization. An interaction range that is too small limits the effective capture of local synchronous joint spatial-temporal correlations, while an excessively large range may introduce noise, thereby affecting model performance. (ii) Encoding vectors with smaller dimensions are sufficient to effectively represent spatial-temporal position and distance information. (iii) STEI-PCN does not require stacking too many TDCNs to achieve optimal performance. When $L = 3$, the effective receptive field is sufficient to cover historical outputs prior to any given timestamp, enabling the model to effectively capture long-range temporal causal correlations.

5.8. Computational cost

Table 5 presents a comparison for prediction horizons of an hour (horizon=12) of STEI-PCN with several advanced baseline models in terms of parameters, training time and inferring time on the smaller-scale dataset PeMS04 and the larger-scale dataset PeMS07. The results show that STEI-PCN maintains a reasonable parameter scale (0.45M or 0.46M) and demonstrates extremely fast per-epoch training and inference speeds. The pure convolutional network architecture of STEI-PCN supports efficient parallel computation, enabling it to exhibit excellent prediction performance even on the large-scale dataset PeMS07, while maintaining high computational efficiency (training and inference time are 107.21 seconds and 1.42 seconds, respectively) and a moderate parameter count (0.46M). Therefore, STEI-PCN is a lightweight model with very low training costs. Its low training cost and exceptional prediction performance give it a significant competitive advantage in traffic prediction tasks.

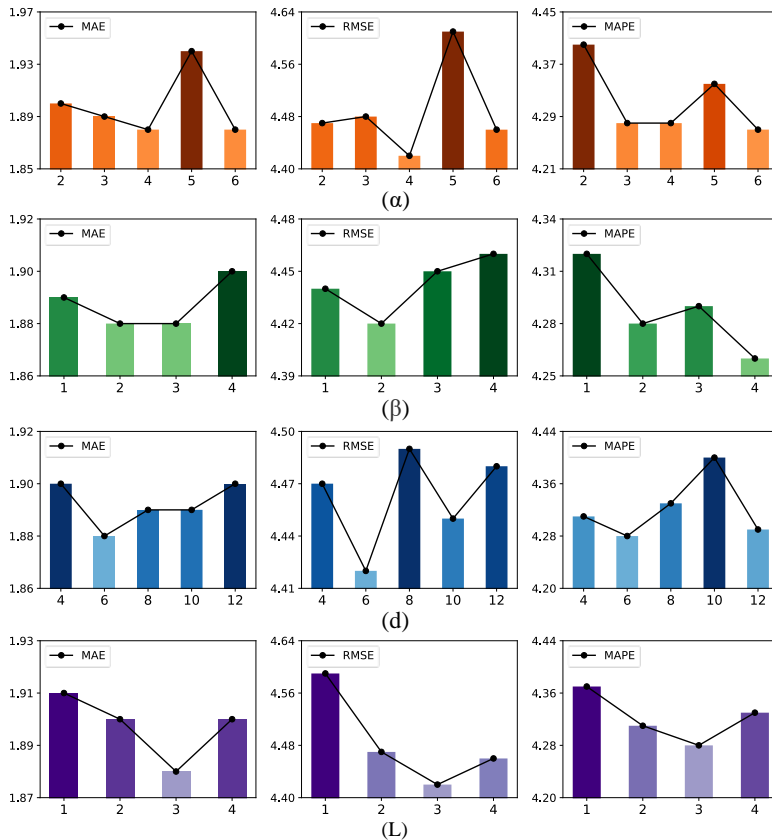


Figure 8: Effects of hyper-parameters on the PeMS-Bay dataset. We study the influence of four hyper-parameters: the size of the spatial-temporal interaction range (α , β), the dimension d of the position embedding, and the number L of TDCNs.

6. Conclusion

This paper proposes an efficient pure convolutional network for traffic prediction via spatial-temporal encoding and inferring (STEI-PCN). The inference module STEI, based on four types of spatial and temporal encodings, is used to adaptively infer the weights of dynamic local synchronous joint spatial-temporal correlations among spatial-temporal neighbors. Given that the generation of encodings relies on the connectivity of the traffic network, there are certain limitations when applied to urban zoning networks, especially irregular zoning networks. Subsequently, the generated dynamic joint spatial-temporal weight matrix is applied to the graph convolutional layer to aggregate and update node features, thereby capturing local synchronous

Model	PeMS04			PeMS07		
	Param.	Train.	Infer.	Param.	Train.	Infer.
DSTAGNN (2022)	3.58	56.74	3.16	14.41	628.65	36.55
STPGCN (2022)	0.20	35.39	1.12	0.20	333.70	15.98
DGCRN (2023)	0.22	21.5	1.16	0.22	138.88	7.72
PDFormer (2023)	0.53	18.37	1.59	0.53	154.31	4.97
SSGCRTN (2024)	0.38	29.23	1.44	0.46	86.76	3.18
STEI-PCN (ours)	0.45	10.94	0.25	0.46	107.21	1.42

Table 5: Models parameters (million) and the cost of training and testing (s/epoch) on PeMS04/08 datasets.

joint spatial-temporal correlations. To preserve the unique patterns of each node, the spatial and temporal coordinates of the nodes are encoded and integrated into the updated features, guiding the GLU to assign differentiated weights to each node’s features. To capture long-range temporal correlations, three layers of TDCN are employed. Finally, through skip connections, we fuse the features from three perspectives activated by GLU to generate comprehensive predictions. Comprehensive experimental results demonstrate that STEI-PCN exhibits significant advantages in computational efficiency and prediction accuracy.

We plan to extend the model in future research from the following aspects: (i) Improving the encoding methods to make them applicable to urban zoning networks, especially irregular zoning networks. (ii) Exploring the application of this model to time series prediction tasks in other domains.

CRedit authorship contribution statement

Kai Hu: Conceptualization, Methodology, Software, Writing- Original draft preparation, Visualization. **Zhifeng Hao:** Writing- Reviewing and Editing, Supervision. **Zhidan Zhao:** Writing- Reviewing and Editing, Supervision.

Declaration of competing interest

The authors declare that they have no conflict of interest.

Data availability

Data will be made available on request.

Acknowledgments

The research was supported by the National Natural Science Foundation of China (Grant No.62476163, 62176148), the National Natural Science Foundation of China (Grants U24A20233), the Guangdong Basic and Applied Basic Research Foundation (2023B1515120020).

References

- [1] Y. Zhou, J. Wang, H. Yang, Resilience of transportation systems: concepts and comprehensive review, *IEEE Transactions on Intelligent Transportation Systems* 20 (12) (2019) 4262–4276, <https://doi.org/10.1109/TITS.2018.2883766>.
- [2] X. Wei, Y. Ren, L. Shen, T. Shu, Exploring the spatiotemporal pattern of traffic congestion performance of large cities in china: A real-time data based investigation, *Environmental Impact Assessment Review* 95 (2022) 106808, <https://doi.org/10.1016/j.eiar.2022.106808>.
- [3] S. Xu, C. Sun, N. Liu, Road congestion and air pollution-analysis of spatial and temporal congestion effects, *Science of the Total Environment* 945 (2024) 173896, <https://doi.org/10.1016/j.scitotenv.2024.173896>.
- [4] A. Rehman, K. Haseeb, T. Saba, J. Lloret, Z. Ahmed, Towards resilient and secure cooperative behavior of intelligent transportation system using sensor technologies, *IEEE Sensors Journal* 22 (7) (2022) 7352–7360, <https://doi.org/10.1109/JSEN.2022.3152808>.
- [5] N. Nigam, D. P. Singh, J. Choudhary, A review of different components of the intelligent traffic management system, *Symmetry* 15 (3) (2023) 583, <https://doi.org/10.3390/sym15030583>.
- [6] T. Garg, G. Kaur, A systematic review on intelligent transport systems, *Journal of Computational and Cognitive Engineering* 2 (3) (2023) 175–188, <http://dx.doi.org/10.47852/bonviewJCCE2202245>.

- [7] A. Háznagy, I. Fi, A. London, T. Nemeth, Complex network analysis of public transportation networks: A comprehensive study, in: 2015 International Conference on Models and Technologies for Intelligent Transportation Systems (MT-ITS), 2015, pp. 371–378, <https://doi.org/10.1109/MTITS.2015.7223282>.
- [8] Z. Tian, L. Jia, H. Dong, F. Su, Z. Zhang, Analysis of urban road traffic network based on complex network, *Procedia Engineering* 137 (2016) 537–546, <https://doi.org/10.1016/j.proeng.2016.01.290>.
- [9] M. Zhang, T. Huang, Z. Guo, Z. He, Complex-network-based traffic network analysis and dynamics: A comprehensive review, *Physica A: Statistical Mechanics and its Applications* 607 (2022) 128063, <https://doi.org/10.1016/j.physa.2022.128063>.
- [10] G. Jin, Y. Liang, Y. Fang, Z. Shao, J. Huang, J. Zhang, Y. Zheng, Spatio-temporal graph neural networks for predictive learning in urban computing: A survey, *IEEE Transactions on Knowledge and Data Engineering* 36 (10) (2023) 5388–5408, <https://doi.org/10.1109/TKDE.2023.3333824>.
- [11] L. Li, X. Su, Y. Zhang, Y. Lin, Z. Li, Trend modeling for traffic time series analysis: An integrated study, *IEEE Transactions on Intelligent Transportation Systems* 16 (6) (2015) 3430–3439, <https://doi.org/10.1109/TITS.2015.2457240>.
- [12] Y. Li, R. Yu, C. Shahabi, Y. Liu, Diffusion convolutional recurrent neural network: Data-driven traffic forecasting, in: International Conference on Learning Representations (ICLR '18), 2018, <https://doi.org/10.48550/arXiv.1707.01926>.
- [13] B. Yu, H. Yin, Z. Zhu, Spatio-temporal graph convolutional networks: A deep learning framework for traffic forecasting, in: Proceedings of the 27th International Joint Conference on Artificial Intelligence (IJCAI), 2018, <https://doi.org/10.24963/ijcai.2018/505>.
- [14] Z. Wu, S. Pan, G. Long, J. Jiang, C. Zhang, Graph wavenet for deep spatial-temporal graph modeling, in: Proceedings of the 28th International Joint Conference on Artificial Intelligence, 2019, pp. 1907–1913, <https://doi.org/10.48550/arXiv.1906.00121>.

- [15] C. Song, Y. Lin, S. Guo, H. Wan, Spatial-temporal synchronous graph convolutional networks: A new framework for spatial-temporal network data forecasting, in: Proceedings of the AAAI Conference on Artificial Intelligence, Vol. 34, 2020, pp. 914–921, <https://doi.org/10.1609/aaai.v34i01.5438>.
- [16] S. Li, L. Ge, Y. Lin, B. Zeng, Adaptive spatial-temporal fusion graph convolutional networks for traffic flow forecasting, in: 2022 International Joint Conference on Neural Networks (IJCNN), IEEE, 2022, pp. 1–8, <https://doi.org/10.1109/IJCNN55064.2022.9892326>.
- [17] H. Y. Bai, X. Liu, T-graphormer: Using transformers for spatiotemporal forecasting, ArXiv Preprint ArXiv: 2501.13274 (2025, <https://doi.org/10.48550/arXiv.2501.13274>).
- [18] X. Fang, J. Huang, F. Wang, L. Zeng, H. Liang, H. Wang, Constgat: Contextual spatial-temporal graph attention network for travel time estimation at baidu maps, in: Proceedings of the 26th ACM SIGKDD International Conference on Knowledge Discovery & Data Mining, 2020, pp. 2697–2705, <http://dx.doi.org/10.1145/3394486.3403320>.
- [19] Y. Zhao, Y. Lin, H. Wen, T. Wei, X. Jin, H. Wan, Spatial-temporal position-aware graph convolution networks for traffic flow forecasting, IEEE Transactions on Intelligent Transportation Systems 24 (8) (2022) 8650–8666, <https://doi.org/10.1109/TITS.2022.3220089>.
- [20] T. Liu, A. Jiang, J. Zhou, M. Li, H. K. Kwan, Graphsage-based dynamic spatial-temporal graph convolutional network for traffic prediction, IEEE Transactions on Intelligent Transportation Systems 24 (10) (2023) 11210–11224, <https://doi.org/10.1109/TITS.2023.3279929>.
- [21] S. Yang, Q. Wu, Y. Wang, T. Lin, Ssgcrtn: a space-specific graph convolutional recurrent transformer network for traffic prediction, Applied Intelligence 54 (22) (2024) 11978–11994, <https://doi.org/10.1007/s10489-024-05815-1>.
- [22] L. Peng, X. Liao, T. Li, X. Guo, X. Wang, An overview based on the overall architecture of traffic forecasting, Data Science and Engineering 9 (3) (2024) 341–359, <https://doi.org/10.1007/s41019-024-00246-x>.

- [23] C. Zheng, X. Fan, C. Wang, J. Qi, Gman: A graph multi-attention network for traffic prediction, in: Proceedings of the AAAI Conference on Artificial Intelligence, Vol. 34, 2020, pp. 1234–1241, <https://doi.org/10.48550/arXiv.1911.08415>.
- [24] J. Jiang, C. Han, W. X. Zhao, J. Wang, Pdformer: Propagation delay-aware dynamic long-range transformer for traffic flow prediction, in: Proceedings of the AAAI Conference on Artificial Intelligence, Vol. 37, 2023, pp. 4365–4373, <https://doi.org/10.1609/aaai.v37i4.25556>.
- [25] W. Shao, Z. Jin, S. Wang, Y. Kang, X. Xiao, H. Menouar, Z. Zhang, J. Zhang, F. Salim, Long-term spatio-temporal forecasting via dynamic multiple-graph attention, in: Proceedings of the Thirty-First International Joint Conference on Artificial Intelligence, IJCAI-22, 2022, pp. 2225–2232, <https://doi.org/10.24963/ijcai.2022/309>.
- [26] S. Bai, J. Z. Kolter, V. Koltun, An empirical evaluation of generic convolutional and recurrent networks for sequence modeling, ArXiv Preprint ArXiv: 1803.01271 (2018) <https://doi.org/10.48550/arXiv.1803.01271>.
- [27] J. Fan, W. Weng, H. Tian, H. Wu, F. Zhu, J. Wu, Rgdan: A random graph diffusion attention network for traffic prediction, Neural Networks 172 (2024) 106093, <https://doi.org/10.1016/j.neunet.2023.106093>.
- [28] W. Jiang, J. Luo, Graph neural network for traffic forecasting: A survey, Expert Systems with Applications 207 (2022) 117921, <https://doi.org/10.1016/j.eswa.2022.117921>.
- [29] S. Guo, Y. Lin, N. Feng, C. Song, H. Wan, Attention based spatial-temporal graph convolutional networks for traffic flow forecasting, in: Proceedings of the AAAI Conference on Artificial Intelligence, Vol. 33, 2019, pp. 922–929, <https://doi.org/10.1609/aaai.v33i01.3301922>.
- [30] Z. Wu, S. Pan, G. Long, J. Jiang, X. Chang, C. Zhang, Connecting the dots: Multivariate time series forecasting with graph neural networks, in: Proceedings of the 26th ACM SIGKDD International Conference on Knowledge Discovery & Data Mining, 2020, pp. 753–763, <https://doi.org/10.48550/arXiv.2005.11650>.
- [31] L. Bai, L. Yao, C. Li, X. Wang, C. Wang, Adaptive graph convolutional recurrent network for traffic forecasting, Advances

- in *Neural Information Processing Systems* 33 (2020) 17804–17815, <https://doi.org/10.48550/arXiv.2007.02842>.
- [32] S. Lan, Y. Ma, W. Huang, W. Wang, H. Yang, P. Li, Dstagnn: Dynamic spatial-temporal aware graph neural network for traffic flow forecasting, in: *International Conference on Machine Learning*, 2022, pp. 11906–11917, <https://api.semanticscholar.org/CorpusID:250340665>.
- [33] F. Li, J. Feng, H. Yan, G. Jin, F. Yang, F. Sun, D. Jin, Y. Li, Dynamic graph convolutional recurrent network for traffic prediction: Benchmark and solution, *ACM Transactions on Knowledge Discovery from Data* 17 (1) (2023) 1–21, <https://doi.org/10.1145/3532611>.
- [34] Y. Chen, I. Segovia, Y. R. Gel, Z-gcnets: Time zigzags at graph convolutional networks for time series forecasting, in: *International Conference on Machine Learning*, 2021, pp. 1684–1694, <https://doi.org/10.48550/arXiv.2105.04100>.
- [35] B.-A. Dai, B.-L. Ye, L. Li, A novel hybrid time-varying graph neural network for traffic flow forecasting, *ArXiv Preprint ArXiv: 2401.10155* (2024, <https://doi.org/10.48550/arXiv.2401.10155>).
- [36] J. Deng, X. Chen, R. Jiang, X. Song, I. W. Tsang, St-norm: Spatial and temporal normalization for multi-variate time series forecasting, in: *Proceedings of the 27th ACM SIGKDD Conference on Knowledge Discovery & Data Mining*, 2021, pp. 269–278, <https://doi.org/10.1145/3447548.3467330>.
- [37] Z. Shao, Z. Zhang, F. Wang, Y. Xu, Pre-training enhanced spatial-temporal graph neural network for multivariate time series forecasting, in: *Proceedings of the 28th ACM SIGKDD Conference on Knowledge Discovery & Data Mining*, 2022, pp. 1567–1577, <https://doi.org/10.1145/3534678.3539396>.
- [38] H. Gao, R. Jiang, Z. Dong, J. Deng, Y. Ma, X. Song, Spatial-temporal-decoupled masked pre-training for spatiotemporal forecasting, in: *Proceedings of the Thirty-Third International Joint Conference on Artificial Intelligence, IJCAI-24*, 2024, pp. 3998–4006, <https://doi.org/10.24963/ijcai.2024/442>.

- [39] Z. Shao, Z. Zhang, F. Wang, W. Wei, Y. Xu, Spatial-temporal identity: A simple yet effective baseline for multivariate time series forecasting, in: Proceedings of the 31st ACM International Conference on Information & Knowledge Management, 2022, pp. 4454–4458, <https://doi.org/10.48550/arXiv.2208.05233>.
- [40] H. Liu, Z. Dong, R. Jiang, J. Deng, J. Deng, Q. Chen, X. Song, Spatio-temporal adaptive embedding makes vanilla transformer sota for traffic forecasting, in: Proceedings of the 32nd ACM International Conference on Information and Knowledge Management, 2023, pp. 4125–4129, <https://doi.org/10.1145/3583780.3615160>.
- [41] J. Chen, H. Ye, Z. Ying, Y. Sun, W. Xu, Dynamic trend fusion module for traffic flow prediction, ArXiv Preprint ArXiv: 2501.10796 (2025, <https://doi.org/10.1016/j.asoc.2025.112979>).
- [42] Y. N. Dauphin, A. Fan, M. Auli, D. Grangier, Language modeling with gated convolutional networks, in: International Conference on Machine Learning, 2017, pp. 933–941, <https://doi.org/10.48550/arXiv.1612.08083>.
- [43] K. He, X. Zhang, S. Ren, J. Sun, Deep residual learning for image recognition, in: Proceedings of the IEEE Conference on Computer Vision and Pattern Recognition, 2016, pp. 770–778, <https://doi.org/10.1109/CVPR.2016.90>.
- [44] Y. Fang, Y. Qin, H. Luo, F. Zhao, B. Xu, L. Zeng, C. Wang, When spatio-temporal meet wavelets: Disentangled traffic forecasting via efficient spectral graph attention networks, in: 2023 IEEE 39th International Conference on Data Engineering (ICDE), 2023, pp. 517–529, <https://doi.org/10.1109/ICDE55515.2023.00046>.